Received: Added at production | Revised: Added at production | Accepted: Added at production

DOI: xxx/xxxx

ARTICLE TYPE

Adaptive integral sliding mode fault-tolerant control for diesel engine air path system via disturbance observer

Wenjie Wu[1] | **Shaoping Wang**[1,2,3] | **Yuwei Zhang**[1] | **Xingjian Wang**[1,2,3] | **Jian Zhang**[4]

[1]School of Automation Science and Electrical Engineering, Beihang University, Beijing, China

[2]Ningbo Institute of Technology, Beihang University, Ningbo, China

[3]Tianmushan Laboratory, Hangzhou, China

[4]Shanghai Marine Diesel Engine Research Institute, Shanghai, China

Correspondence

*Shaoping Wang, School of Automation Science and Electrical Engineering, Beihang University, Beijing.

Email: shaopingwang@vip.sina.com

Abstract

This paper proposes a fault-tolerant control strategy for the air path system of a turbocharged diesel engine, considering the simultaneous presence of matched and mismatched external disturbances, additive and loss of effectiveness fault modes in the EGR and VGT subsystems. Firstly, a disturbance observer based on H_∞ theory is designed for estimating additive faults and external disturbances, and the upper bound of observation error is obtained. Based on the observation information, an integral sliding mode surface is designed, and the effectiveness of the sliding mode surface is analyzed. For the loss of effectiveness faults in the actuators, a novel adaptive update sliding mode controller is designed. The proposed control algorithm can get the fault information of the system and achieve fault-tolerant control of through controller reconstruction. Ultimately, the effectiveness of the proposed method is validated through simulations and comparative analysis.

KEYWORDS

fault tolerant control; diesel engine air path; disturbance observer; sliding mode control; adaptive update

1 | INTRODUCTION

Compared to gasoline engines, diesel engines have advantages such as high thermal efficiency, low power-to-weight ratio, high energy utilization efficiency, and low carbon dioxide emissions. However, due to the emissions primarily consisting of NO_x and soot, diesel engines still pose environmental challenges. To achieve emission reduction goals for diesel engines, many researchers have conducted relevant studies(1–5). Among them, coordinating the exhaust gas recirculation (EGR) and variable geometry turbocharger (VGT) actuators in the diesel engine air path (DEAP) system to control the intake and exhaust states of the cylinders and optimize the in-cylinder combustion process has proven to be an effective measure(6–10).

Due to the strong coupling between the EGR and VGT actuators, it is necessary to establish a mathematical model for the DEAP system in order to achieve control. Many scholars have therefore developed mathematical models for the DEAP system and designed various control algorithms based on these models(11–16). Aiming at the modeling and control of diesel engine in (11), an overview of model of diesel engine is proposed. The simulations indicate that the model and control method have achieved a certain level of accuracy. Based on the conservation of mass and energy law and the ideal gas law, a general DEAP model is proposed in (15). A controller is then designed based on the Lyapunov function. In (13) and (12), the Model Predictive Control (MPC) method is applied to the DEAP control problem. Due to the nonlinearity of the DEAP model, different techniques are used to handle the nonlinearity in the model. A singular perturbation control method is proposed in (14) for a dual-loop (high-pressure loop and low-pressure loop) EGR DEAP system. The effectiveness of the method is validated through experiments. In (16), to address the issue of input saturation in DEAP system, a adaptive robust controller is designed by incorporating an auxiliary system to compensate for the effects of saturation.

To enhance the reliability of the DEAP system, fault-tolerant control algorithms specifically designed for this system have emerged(17–21). In (17), the super-twisting algorithm is used to address the situation where both additive faults and loss of effectiveness (LOE) faults coexist in the DEAP system. Similarly, in (20), the combination of an extended state observer and the super-twisting algorithm is employed to achieve precise tracking of the desired state in the presence of similar fault scenarios.

Abbreviations: DEAP, diesel engine air path; EGR, exhaust gas recirculation; VGT, variable geometry turbocharger; LOE, loss of effectiveness; DO, disturbance observer.

By transforming the complex nonlinear DEAP model into a T-S fuzzy model, a control strategy is developed in (18) to address leakage and sensor faults in the DEAP system. This strategy combines parallel distributed compensation control and MPC design. When dealing with both matched and mismatched disturbances in DEAP systems, (19) introduces an adaptive super-twisting extended state observer, built upon the foundation of the sliding mode control algorithm. In consideration of the aforementioned issues where the DEAP system faces the presence of matched disturbances, system uncertainties, LOE faults, and additive faults simultaneously, (21) proposes an adaptive sliding mode control method based on a disturbance observer. However, this method still cannot address the case of mismatched disturbances.

From the above, it can be seen that the current problem of simultaneously dealing with matched and mismatched disturbances, additive and LOE faults in DEAP systems remains an open issue. Furthermore, the aforementioned methods belong to passive fault-tolerant control, which means that they handle actuator faults through the robustness of the control algorithms themselves. Therefore, when dealing with actuator faults, these methods may have certain limitations or deficiencies in terms of performance.

In order to solve the above control problems, the relevant literature was investigated(22–32),. Sliding mode control, known for its robustness against external disturbances and system uncertainties, has been extensively employed by researchers in the design of fault-tolerant control methods. To concurrently manage matched and mismatched disturbances within the system, a novel sliding mode control design methodology was introduced in the paper (26). This method incorporates the observations from the disturbance observer and achieves excellent performance. In (27), the unmanned marine vehicle (UMV) model was transformed into a T-S fuzzy model. Considering the possibility of two fault modes in the model, an adaptive fuzzy sliding mode controller was designed to achieve dynamic position control of the UMV. In (28), an innovative adaptive sliding mode controller has been designed to stabilize a T-S fuzzy singular Markovian jump system with uncertain transition rates. This design takes into account the presence of actuator faults and parameter uncertainty within the model. For manipulator systems, both (29) and (30) design fault-tolerant controllers based on the sliding mode method. The difference is that (29) proposes an integral sliding manifold technology based on auxiliary functions, which can fully eliminate the influence of system uncertainties; while (30) makes the system more stable by using sliding mode observer technology. (31) proposes a fault-tolerant controller based on adaptive sliding mode for quadrotor unmanned aerial. This method introduces the boundary layer in the sliding mode controller, thereby effectively avoiding overshoot of the parameter estimate and chattering of the controller.

Considering the aforementioned overview, it can be deduced that the utilization of fault-tolerant control techniques founded on sliding mode control has attained extensive recognition and shown its effectiveness. Thus, building upon the H_∞ theory, this paper introduces a fault-tolerant adaptive sliding mode controller for the DEAP system, incorporating a disturbance observer. In comparison with previous studies, the primary contributions of this paper are as follows:

• To achieve fault-tolerant control in DEAP systems, a novel adaptive integral sliding mode controller based on disturbance observer is proposed. This controller has a relatively simple structure but is capable of simultaneously handling external matched and mismatched disturbances, as well as additive and LOE faults in the system. To the best of our knowledge(17–21), this is the first controller designed specifically for DEAP systems that can address the simultaneous occurrence of the aforementioned conditions.

• Based on the disturbance observer, we can obtain information about additive faults and external disturbances, which is then incorporated into the design of the sliding mode surface. By using adaptive update laws, the estimation of LOE faults can be obtained. The advantage of this design lies in its ability to estimate actuator faults, monitor the health status of the actuators online, and reconstruct the controller structure, thereby achieving better fault-tolerant control performance for DEAP systems.

The paper is organized as follows. Section 2 introduces the DEAP model and fuzzifies the model, and then introduces the external disturbance and actuator fault models. Section 3 first introduces the design of the disturbance observer. A novel integral sliding mode surface based on disturbance estimation is designed. Finally, a new adaptive sliding mode controller is designed. Simulation results are given in Section 4.

Notations: $\| * \| = \sqrt{*^T *}$ denotes the Euclidean-norm. $\mathbf{I}^n$ represents a n-dimensional unit vector. $\mathbf{He}\{*\} = * + *^T$. $\star$ denotes the transpose of the corresponding block matrix.

2 | PROBLEM STATEMENT

2.1 | Mathematical model of DEAP

The diesel engine air path system (DEAP) model is illustrated in Figure 1. The structure of the diesel engine air system primarily encompasses components such as the exhaust gas re-circulation (EGR) system, variable geometry turbocharger (VGT) system,

compressor, and inter-cooler. As evident from the diagram, alterations to the gas state within the intake and exhaust manifolds can be induced by the EGR and VGT, and a coupling effect exists between the EGR and VGT. To ensure precise and decoupled control of the gas state, a suitable mathematical model is requisite, and corresponding control algorithms must be devised to accomplish this goal.

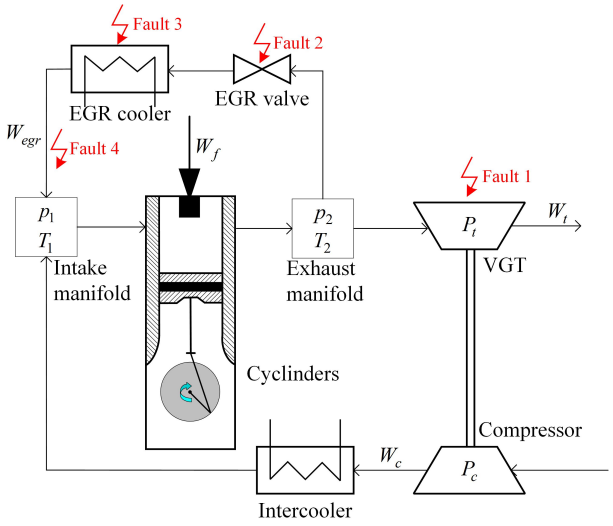

FIGURE 1 DEAP system with typical faults

A third order mode established in (15) is usually used to describe the DEAP system:

$$\begin{aligned}
\dot{p}_1 &= k_1(W_c + W_{egr} - k_e p_1) + \frac{\dot{T}_1}{T_1} p_1 \\
\dot{p}_2 &= k_2(k_e p_1 - W_{egr} - W_t + W_f) + \frac{\dot{T}_2}{T_2} p_2 \\
\dot{P}_c &= \frac{1}{\tau}(\eta_m P_t - P_c)
\end{aligned} \tag{1}$$

here, the compressor and turbine mass flow rates, denoted as W_c and W_t respectively, exhibit a relationship with the compressor and turbine power, represented as P_c and P_t respectively, through the following correlation:

$$\begin{aligned}
W_c &= P_c \frac{k_c}{p_1^{\mu} - 1} \\
P_t &= k_t(1 - p_2^{-\mu}) W_t
\end{aligned} \tag{2}$$

where :

$$\begin{aligned}
k_c &= \frac{\eta_c}{c_p T_a},\ k_t = c_p \eta_t T_2,\ k_1 = \frac{R_a T_1}{V_1}, \\
k_e &= \frac{\eta_v N V_d}{R_a T_1},\ k_2 = \frac{R_a T_2}{V_2}
\end{aligned}$$

In order to facilitate viewing, the meaning of diesel engine variables are shown in Table 1.

For diesel engines, the change of T_1 and T_2 is usually very slow, so the model parameters $(k_1, k_2, k_c, k_e, k_t)$ are usually taken as constants(17–21; 33). In order to facilitate the design of the controller in this article, according to the literature (18), the model (1) can be constructed as the following T-S fuzzy form through the sector nonlinear modeling approach:

$$\dot{x} = \sum_{i=1}^{4} h_i \left(A_i x + B_i u + B_d d\right) \tag{3}$$

TABLE 1 Meaning of diesel engine variables in this paper.

Variables	Meaning	Units
p_1	Intake manifold pressure	*bar*
p_2	Exhaust manifold pressure	*bar*
P_c	Compressor power	*W*
P_t	Turbine power	*W*
T_1	Intake manifold temperature	*K*
T_2	Exhaust manifold temperature	*K*
T_a	Ambient temperature	*K*
W_{egr}	EGR mass flow	*Kg/s*
W_t	VGT mass flow	*Kg/s*
W_f	Fueling mass flow rate	*Kg/s*
c_p	Specific heat at constant pressure	*J/(Kg.K)*
η_v	Engine volumetric efficiency	–
η_c	Compressor isentropic efficiency	–
η_t	Engine volumetric efficiency	–
V_1	Intake manifold volume	m^3
V_2	Exhaust manifold volume	m^3
V_d	Engine Volume cylinder	m^3
R_a	Specific gas constant	*J/(Kg.K)*

where $x = \begin{bmatrix} p_1 & p_2 & P_c \end{bmatrix}^T$, $u = \begin{bmatrix} W_{egr} & W_t \end{bmatrix}^T$, $d \in \mathrm{R}^m$ is the mismatched disturbance, $B_d \in \mathrm{R}^{3\times m}$ is the disturbance matrix,

$$A_{i=\{1,2\}} = \begin{bmatrix} -k_1 k_e & 0 & k_1 k_c \underline{\beta}_1 \\ k_2 k_e & 0 & 0 \\ 0 & 0 & \frac{-1}{\tau} \end{bmatrix}, B_{i=\{2,4\}} = \begin{bmatrix} k_1 & 0 \\ -k_2 & -k_2 \\ 0 & k_t \overline{\beta}_2 \end{bmatrix}, h_1 = \frac{(\overline{\beta}_1 - \beta_1)(\overline{\beta}_2 - \beta_2)}{(\overline{\beta}_1 - \underline{\beta}_1)(\overline{\beta}_2 - \underline{\beta}_2)},\ h_2 = \frac{(\overline{\beta}_1 - \beta_1)(\beta_2 - \underline{\beta}_2)}{(\overline{\beta}_1 - \underline{\beta}_1)(\overline{\beta}_2 - \underline{\beta}_2)}$$

$$A_{i=\{3,4\}} = \begin{bmatrix} -k_1 k_e & 0 & k_1 k_c \overline{\beta}_1 \\ k_2 k_e & 0 & 0 \\ 0 & 0 & \frac{-1}{\tau} \end{bmatrix}, B_{i=\{1,3\}} = \begin{bmatrix} k_1 & 0 \\ -k_2 & -k_2 \\ 0 & k_t \underline{\beta}_2 \end{bmatrix}, h_3 = \frac{(\beta_1 - \underline{\beta}_1)(\overline{\beta}_2 - \beta_2)}{(\overline{\beta}_1 - \underline{\beta}_1)(\overline{\beta}_2 - \underline{\beta}_2)},\ h_4 = \frac{(\beta_1 - \underline{\beta}_1)(\beta_2 - \underline{\beta}_2)}{(\overline{\beta}_1 - \underline{\beta}_1)(\overline{\beta}_2 - \underline{\beta}_2)}$$

$$d = \begin{bmatrix} \frac{\dot{T}_1}{T_1} p_1 & \frac{\dot{T}_2}{T_2} p_2 + W_f \end{bmatrix}^T$$

β_1 and β_2 are the premise variables, $\beta_1 = \frac{1}{p_1^{\mu}-1}$ and $\beta_2 = 1 - p_2^{-\mu}$, $\overline{\beta}_i$ and $\underline{\beta}_i$ are the upper and lower bounds of β_i.

Remark 1. In the DEAP model, in order to facilitate the design of the control law, W_{egr} and W_t are taken as input variables. This is possible because the distribution of the required mass flow value can be achieved by manipulating the EGR and VGT systems(15).

Remark 2. For the diesel engine, the variables W_f, T_1, T_2 always change slowly. Hence this terms can be considered as disturbances. During actual operation or simulation, the diesel engine will be subject to other external disturbances, so d can include other terms as well.

2.2 | Typical faults and DEAP model establishment with actuator faults

2.2.1 | Typical faults of VGT and EGR subsystem

W_t and W_{egr} are used as the input variables of model (1), which can be assigned by manipulating the EGR and VGT subsystems, respectively. The VGT and EGR subsystems are both high-frequency failure subsystems in turbocharged diesel engines, and common faults are annotated in Figure 1. Below are descriptions of several common faults:

• **EGR system**

a). LOE faults—As shown in Figure 1, when there is a leakage in the pipeline (Fault 4) or a blockage in the EGR cooler (Fault 3), it will lead to a decrease in gas flow, indicating the occurrence of a LOE fault.

b). Additive faults—The occurrence of EGR valve sticking (Fault 2) will lead to an additive fault in the control input.

The EGR system may also encounter other types of faults that affect the value of W_{egr} (ie, the control variable u_1).

•VGT system

a). LOE faults—During usage, if the compressor blades of the VGT system accumulate dust over a long period without cleaning, it can lead to blade damage and friction with the casing, resulting in a decrease in the efficiency of the VGT system.

b). Additive faults—The turbine intake and exhaust pipes are often prone to blockages caused by impurities such as oil and dust, leading to increased flow resistance in the pipes and resulting in deviations in control inputs from the target values.

Similarly, the VGT system may also encounter other types of faults, and these faults will affect the value of W_t (ie, the control variable u_2).

2.2.2 | DEAP model with faults

Based on the analysis in the previous subsection, it is evident that various types of faults may occur in the EGR and VGT subsystems during the operation of the diesel engine. The input variables (u_1 and u_2) of the DEAP model are directly manipulated by the EGR and VGT subsystems. When the above-mentioned faults occur, the DEAP model considering faults can be established in the following form:

$$\begin{aligned} \dot{x} &= \sum_{i=1}^{4} h_i \left[A_i x + B_i \left(Eu + F_u\right) + B_d d\right] \\ z &= Cx \end{aligned} \tag{4}$$

where $E = diag\left\{e_1, e_2\right\}$ represents the LOE fault, $0 < e_i \leq 1$, $i = \{1, 2\}$, F_u represents the additive fault, z is an adjustable output.

Remark 3. The effectiveness coefficients $e_i > 0$ is a reasonable condition. $e_i = 0$ means that the controller u_i is completely failed. The complete failure of some controllers (i.e. $e_i = 0$) was discussed in our previous research(34).

Assumption 1. The derivative of the disturbance, $\dot{d}$, and the derivative of the additive fault, $\dot{F}_u$, are bounded, and the upper bounds are known.

Remark 4. It needs to be emphasized that the conditions set in Assumption 1 are aimed at providing a rigorous stability analysis. In common controller designs based on disturbance observers(26; 35), it is usually required that both the disturbance d and $\dot{d}$ are bounded, which is also a technical challenge in the field of disturbance observer-based control. However, Assumption 1 only requires that $\dot{d}$ is bounded, which relaxes the requirements for disturbances to some extent. Furthermore, for the disturbances and faults faced by diesel engines, the requirements of Assumption 1 can generally be met(17; 19).

3 | FAULT TOLERANT CONTROLLER DESIGN

In this section, an enhanced disturbance observer (DO) is employed to accurately estimate external disturbances and additive faults originating from the actuators. For the LOE faults of the actuators, robust H_∞ technical based ISMC and adaptive update law are used to eliminate the bad effects. In order to provide a clear depiction of the control structure in this paper, the control block diagram is illustrated in Figure 2.

3.1 | Disturbance observer

For the presence of disturbance and bias faults in system (4), a DO is designed to compensate it. To facilitate the design of DO, system (4) is varied to the following form

$$\dot{x} = \sum_{i=1}^{4} h_i \left(A_i x + B_i E u + D\right) \tag{5}$$

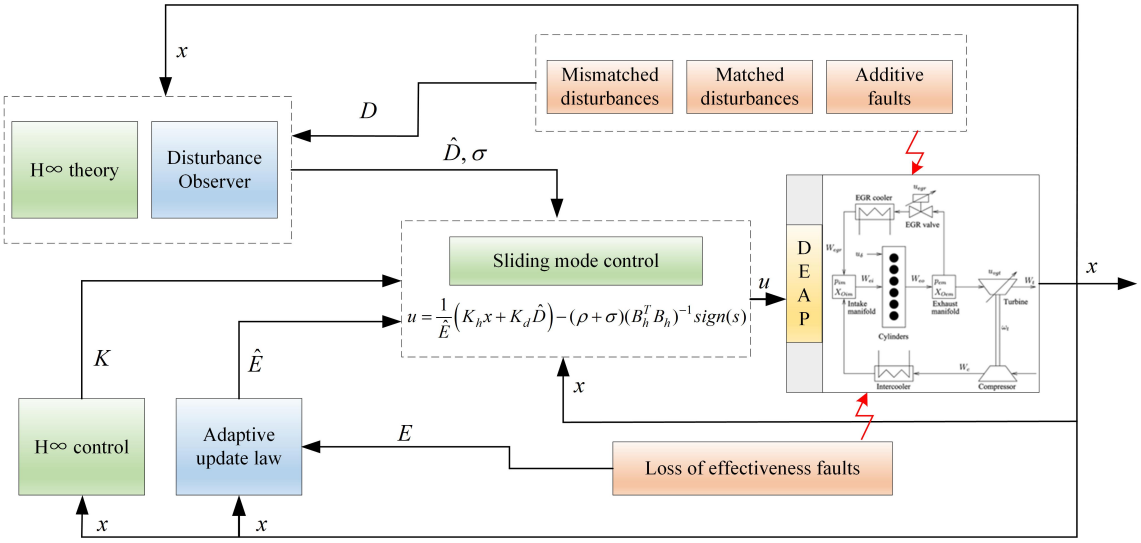

FIGURE 2 Control system scheme

where $D = \sum_{i=1}^{4} h_i B_i F_u + B_d d$. In order to observer D and design the fault-tolerant controller, the following disturbance observer (DO) is designed

$$\begin{aligned} \dot{v} &= \sum_{i=1}^{4} h_i L \left(\hat{D} + A_i x + B_i u\right) \\ \hat{D} &= v - Lx \end{aligned} \tag{6}$$

where L represents the observer gain matrix that requires careful design. Define $e_D = D - \hat{D}$, then consider the system (5) and (6), DO error system can be get:

$$\begin{aligned} \dot{e}_D =& \dot{D} - \dot{\hat{D}} \\ =& \dot{D} - \sum_{i=1}^{4} h_i L \left[\hat{D} + A_i x + B_i u - (A_i x + B_i E u + D)\right] \\ =& L e_D + \omega_D \end{aligned} \tag{7}$$

where $\Delta E = E - \mathbf{I}$, $\omega_D = \sum_{i=1}^{4} h_i L B_i \Delta E u + \dot{D}$.

Theorem 1. The system (7) is asymptotically stable and H_∞ index $\|e_D\| \leq \gamma_o \|\omega_D\|$ is satisfied if there exists invertible matrice $N \in \mathbf{R}^{3\times 3}$ such that the following LMI condition is hold:

$$\begin{bmatrix} N + N^T & P_D & \mathbf{I} \\ \star & -\gamma^2{}_o \mathbf{I} & 0 \\ \star & \star & -\mathbf{I} \end{bmatrix} < 0 \tag{8}$$

where $L = P_D^{-1} N$.

Proof: Define $P_D > 0$, and a Lyapunov function $V_D = e_D^T P_D e_D$ is given, then the derivative of V_D can be obtained as:

$$\dot{V}_D = e_D^T \left(P_D L + L^T P_D\right) e_D + e_D^T P_D \omega_D + \omega_D^T P_D e_D \tag{9}$$

Then the H_∞ index J_D is given as:

$$\begin{aligned} J_D &= \int_0^T \left(e_D^T e_D - \gamma_o^2 \omega_D^T \omega_D + \dot{V}_D\right) dt - V_{DT} \\ &= \int_0^T \left[e_D^T e_D - \gamma_o^2 \omega_D^T \omega_D + e_D^T \left(P_D L + L^T P_D\right) e_D + e_D^T P_D \omega_D + \omega_D^T P_D e_D\right] dt - V_{DT} \end{aligned} \tag{10}$$

where V_{DT} is the value of V_D at time T. By using Schur complement, one can see that $\int_0^T \|e_D\|^2 < \gamma^2 \int_0^T \|\omega_D\|^2$ will hold if the condition (8) is satisfied. This completes the proof. □

According to assumption 1, it can be concluded that $\dot{D}$ is bounded. For DEAP system, the control input u is also bounded. Obviously, it can be concluded that ω_D is bounded. Therefore, based on Theorem 1, it can be concluded that $\|e_D\| \leq \gamma_o \bar{\omega}_D$. $\bar{\omega}_D$ is the upper bound of $\|\omega_D\|$.

3.2 | DO based sliding mode surface

In order to achieve FTC and eliminate the effects of disturbances, effectiveness faults and bias faults at the same time for system (5), motivated by (26), the sliding mode surface is designed as

$$\begin{aligned} s = &- \left(\sum_{i=1}^{4} h_i(\beta_0) B_i\right)^T x_0 + \left(\sum_{i=1}^{4} h_i B_i\right)^T \left\{ x - \int_0^t \sum_{i=1}^{4} \sum_{j=1}^{4} h_i h_j \left[A_i x + B_i \left(K_j x + K_d \hat{D} \right) \right.\right. \\ &\left.\left. + \hat{D} + \left(\sum_{i=1}^{4} \dot{h}_i B_i\right)^T \right] \right\} ds \end{aligned} \tag{11}$$

where $\beta_0 = \beta(0)$, $x_0 = x(0)$, $K_j \in \mathrm{R}^{2\times 3}$ are the control gain matrices, $K_d \in \mathrm{R}^{2\times 3}$ is the disturbance inject matrix. Based on the fault system (5) and sliding mode surface (11), one has:

$$\dot{s} = \left(\sum_{i=1}^{4} h_i B_i\right)^T \left[\sum_{i=1}^{4} \sum_{i=j}^{4} h_i h_j \left(B_i E u - B_i K_j x - B_i K_d \hat{D} \right) + \tilde{D} \right] \tag{12}$$

where $\tilde{D} = D - \hat{D}$. Then sliding mode equivalent control can be get by setting $s = 0$ and $\dot{s} = 0$:

$$u_{eq} = E^{-1} \left(K_h x + K_d \hat{D} - B^{\dagger} \tilde{D} \right) \tag{13}$$

where $B^{\dagger} = \left(B_h^T B_h\right)^{-1} B_h^T$, $\Delta_h = \sum_{i=1}^{4} h_i \Delta_i^T$. Substituting (13) into (5), closed loop system can be get:

$$\dot{x} = (A_h + B_h K_h) x + B_h K_d \hat{D} - B_h B^{\dagger} \tilde{D} + D \tag{14}$$

By letting $K_d = -B^{\dagger}$, one has:

$$\begin{aligned} \dot{x} &= (A_h + B_h K_h) x - B_h B^{\dagger} \left(\hat{D} + \tilde{D} \right) + D \\ &= (A_h + B_h K_h) x + \left(I - B_h B^{\dagger} \right) D \\ &= (A_h + B_h K_h) x + B_d^{\dagger} D \end{aligned} \tag{15}$$

where $B_d^{\dagger} = B_h^{\perp} B^{\perp\dagger}$, $B_h^{\perp} \in \mathrm{R}^{3\times 1}$ is the null space of B_h^T, that is, $B_h^T B_h^{\perp} = 0$, $B^{\perp\dagger} = \left(B_h^{\perp T} B_h^{\perp}\right)^{-1} B_h^{\perp T}$.

Theorem 2. For $\forall i, j, k, m = 1, ..., 4$, the closed loop system (15) is asymptotically stable and H_∞ index $\|z\| \leq \gamma_c \|D\|$ is satisfied if there exists invertible matrices $P_c = P_c^T > 0 \in \mathbf{R}^{3\times 3}$, $M_i \in \mathbf{R}^{2\times 3}$ such that the following LMI conditions are hold:

$$\begin{bmatrix} \mathbf{He}\{A_i P_c + B_i M_j\} & B_i^{\perp} \left(B_j^{\perp T} B_k^{\perp}\right)^{-1} B_m^{\perp T} & P_c C^T \\ \star & -\gamma_c & 0 \\ \star & \star & -\mathbf{I} \end{bmatrix} < 0 \tag{16}$$

where $K_i = M_i * X^{-1}$.

Proof: Define $P_c > 0$, and construct the Lyapunov function as $V = x^T P_c x$, then the derivative of V can be obtained and the H_∞ index J_c can be deduced as:

$$\begin{aligned} J_c &= \int_0^T \left(z^T z - \gamma_c^2 D^T D + \dot{V}\right) dt - V_T \\ &= \int_0^T \left[z^T z - \gamma_c^2 D^T D + x^T \mathbf{He}\{P_c A_h + P_c B_h K_h\} x + x^T P_c B_d^\dagger D + D^T B_d^{\dagger T} P_c x\right] dt - V_T \end{aligned} \tag{17}$$

By using Schur complement, one can see that $\int_0^T \|z\|^2 dt < \gamma_c^2 \int_0^T \|D\|^2 dt$ will hold if the flowing condition is satisfied:

$$\begin{bmatrix} \mathbf{He}\{P_c A_h + P_c B_h K_h\} & P_c B_d^\dagger & C^T \\ \star & -\gamma_c \mathbf{I} & 0 \\ \star & \star & -\mathbf{I} \end{bmatrix} < 0 \tag{18}$$

then pre and post-multiply (18) by $diag\{P_c; \mathbf{I}; \mathbf{I}\}$ and its transpose respectively, and defuzzifying it, the conditions (16) can be get. This completes the proof. □

From Theorem 2, it can be concluded that the sliding surface designed in this paper can make the system asymptotically stable and satisfy the H_∞ performance. Next, the sliding mode controller needs to be designed so that the system converges to the sliding mode surface.

3.3 | Adaptive sliding mode controller design

In order to cope with the effectiveness failure of the DEAP system (5) and to converge to the sliding mode surface, a novel sliding mode controller will be designed in this section.

Based on the Lyapunov theory, the controller is designed as:

$$u = \frac{1}{\hat{E}} \left(K_h x + K_d \hat{D}\right) - (\rho + \sigma)(B_h^T B_h)^{-1} sign(s) \tag{19}$$

where $\hat{E} = diag\{\hat{e}_1; \hat{e}_2\}$ is the estimate of E, ρ is the adjustable parameter, $\sigma = \gamma_o \bar{\omega}_D \|B_h\| / E_{min}$, $E_{min} = min\{e_1\ e_2\}$. Base on the controller (19), the adaptive update law of $\hat{E}$ is proposed:

$$\dot{\hat{e}}_1 = \frac{1}{\hat{e}_1} s^T B_h^T B_h [K_h x + K_d \hat{D}]_1 \tag{20}$$

$$\dot{\hat{e}}_2 = \frac{1}{\hat{e}_2} s^T B_h^T B_h [K_h x + K_d \hat{D}]_2 \tag{21}$$

where

$$[K_h x + K_d \hat{D}]_1 = \begin{bmatrix} \Xi_1 \\ 0 \end{bmatrix}, [K_h x + K_d \hat{D}]_2 = \begin{bmatrix} 0 \\ \Xi_2 \end{bmatrix},$$

Ξ_1 and Ξ_2 are the elements of the first and second row of the vector $[K_h x + K_d \hat{D}]$, respectively.

Theorem 3. Considering the DEAP system (4), by adopting sliding mode controller (19) with adaptive update rate (20)-(21), along with the incorporation of disturbance observer (7), the system will converge to the sliding mode surface (11).

Proof: Since $K_d = -B^\dagger$, combined with the controller (19), the sliding mode dynamic system (12) can be written as

$$\dot{s} = B_h^T B_h E \left[\frac{1}{\hat{E}} \left(K_h x - B^\dagger \hat{D}\right) - (\rho + \sigma)(B_h^T B_h)^{-1} sign(s)\right] - B_h^T B_h K_h x + B_h^T D \tag{22}$$

Consider a Lyapunov function:

$$V_s = \frac{1}{2}(s^T s + \tilde{e}_1^2 + \tilde{e}_2^2) \tag{23}$$

TABLE 2 Reference values for DEAP

variables	reference vale 1	reference vale 2
p_1	2.174	1.2955
p_2	2.87	1.35
P_c	6.97	5.21

where $\tilde{e}_1 = \hat{e}_1 - e_1$, $\tilde{e}_2 = \hat{e}_2 - e_2$. Considering the adaptive law (20)-(21) and the sliding mode dynamic system (22), the derivative of V_s is derived as:

$$\begin{aligned}
\dot{V}_s =& s^T\dot{s} + \tilde{e}_1\dot{\hat{e}}_1 + \tilde{e}_2\dot{\hat{e}}_2 \\
=& s^T B_h^T B_h \frac{E}{\hat{E}}\left(K_h x - B^\dagger \hat{D}\right) - s^T(\rho+\sigma)Esign(s) - s^T\left(B_h^T B_h K_h x - B_h^T D\right) + \frac{\tilde{e}_1}{\hat{e}_1} s^T B_h^T B_h [K_h x \\
& - B^\dagger \hat{D}]_1 + \frac{\tilde{e}_2}{\hat{e}_2} s^T B_h^T B_h [K_h x - B^\dagger \hat{D}]_2 \\
=& s^T B_h^T B_h \frac{E}{\hat{E}}\left(K_h x - B^\dagger \hat{D}\right) - s^T(\rho+\sigma)Esign(s) - s^T\left(B_h^T B_h K_h x - B_h^T D\right) + s^T B_h^T B_h \frac{\hat{E}-E}{\hat{E}}\left(K_h x - B^\dagger \hat{D}\right) \\
=& s^T B_h^T B_h \left(K_h x - B^\dagger \hat{D}\right) - (\rho+\sigma)\|s^T E\| - s^T\left(B_h^T B_h K_h x - B_h^T D\right) \\
=& s^T B_h^T e_D - (\rho+\sigma)\|s^T E\| \\
\leq& \|s^T B_h^T e_D\| - (\rho+\sigma)\|s^T E
\end{aligned} \tag{24}$$

Then, by adopting the results of Theorem 1 and $\sigma = \gamma_o \bar{\omega}_D \|B_h\|/E_{min}$, one has:

$$\begin{aligned}
\dot{V}_s \leq& \|s^T B_h^T \gamma_o \bar{\omega}_D\| - \|s^T B_h^T E/E_{min}\gamma_o \bar{\omega}_D\| - \rho\|s^T E\| \\
\leq& -\rho\|s^T E\| \\
<& 0
\end{aligned} \tag{25}$$

Therefore, the sliding mode surface will converge to 0. This completes the proof. □

4 | SIMULATION AND ANALYSIS

In this section, the validity of the method proposed in this paper will be verified through various simulation examples using the MATLAB software. According to (33), the values of the parameters in system 2 are as follows: $k_1 = 143.91$, $k_2 = 1715.5$, $k_t = 391.365$, $k_e = 0.028$, $k_c = 0.0025$, $\eta_m = 0.95$, $\tau = 0.15$, $\mu = 0.285$, $1.2 \leq p_1 \leq 2$, $1.3 \leq p_2 \leq 4$. Furthermore, based on different operational conditions of the diesel engine, two distinct target states have been given, as illustrated in Table 2.

According to the control method designed in this paper, the first step is to solve the disturbance observer based on Theorem 1, in order to obtain the observer gain matrix and the H_∞ index γ_o. By solving inequality (6), it can be concluded that $\gamma_o = 0.0055$, and

$$L = \begin{bmatrix} -24.7487 & 0 & 0 \\ 0 & -24.7487 & 0 \\ 0 & 0 & -24.7487 \end{bmatrix}$$

The second step is to design the sliding surface. According to Theorem 2, the feedback gain matrices K_i can be obtained:

$$K_1 = \begin{bmatrix} 528.081666624847 & -639.742654076265 \\ 37.8166307464728 & -45.7703584474523 \\ 337.866854113481 & -409.348310361652 \end{bmatrix}^T$$

$$K_2 = \begin{bmatrix} 528.081666624358 & -639.742654075903 \\ 37.8166307464377 & -45.7703584474263 \\ 337.866854113168 & -409.348310361421 \end{bmatrix}^T$$

$$K_3 = \begin{bmatrix} 528.081666624697 & -639.742654076018 \\ 37.8166307464619 & -45.7703584474345 \\ 337.866854113385 & -409.348310361494 \end{bmatrix}^T$$

$$K_4 = \begin{bmatrix} 528.081666624406 & -639.742654075819 \\ 37.8166307464412 & -45.7703584474204 \\ 337.866854113199 & -409.348310361367 \end{bmatrix}^T$$

and $\gamma_c = 0.5164$. In order to reduce the chattering phenomenon in the sliding mode control process, a common method is used to replace the sign function (36):

$$sign(s) = \frac{s}{|s| + \rho}$$

where ρ is a small scalar, here the value is $\rho = 0.01$.

Case 1: Performance of system with LOE faults and additive faults

In this case, it is assumed that the controller has LOE faults and additive faults at the same time, and there is no external disturbance. The control method for similar problems is also given in (21). In order to verify the superiority of the method in this paper, the simulation results will be compared and analyzed. It is assumed that there is a LOE fault as shown below during execution:

$$E(t) = \begin{cases} 0.65 + 0.05\sin(0.01t) \times \mathbf{I}_{2\times 2} & t > 15s \\ \mathbf{I}_{2\times 2} & 0 \le t \le 15s \end{cases}$$

and additive fault is given as:

$$F_u = [0.05\sin(0.8t), 0.06\cos(0.8t) + e^{-t}\sin(t)]^T$$

Assuming the existence of the aforementioned actuator faults in the system, figure 3 shows the sliding mode response curve. It can be seen from the figure that when the system states start to switch, the sliding mode surface will have a slight jump, but it will stabilize in about 1-2s. When the LOE fault occurs at 15 seconds, indicating a change in system parameters, the sliding mode surface will experience relatively large jumps. However, due to the presence of adaptive update laws, the sliding mode surface can still return to a stable state within a short period of time.

The estimated value curves of the controller's LOE fault coefficient are shown in the figure 4. It can be seen that when no LOE fault occurs before 15s, that is, the failure coefficient is 1, the accurate estimation of the LOE fault can be realized through the adaptive update rate. When the system state is switched at 10s, due to chattering on the sliding mode surface, the estimated value of the LOE fault coefficient will chatter to a small extent, but it will return to the real value in a short time. At 15 seconds, it is assumed that the system controller suffers a sudden LOE fault, and this fault coefficient changes slowly over time. According to the simulation results, it can be seen that even if a sudden failure occurs, the estimated value of the fault coefficient can track the real value in a short time. When the system state switches in the 20s and 30s, the estimated fault value will chatter slightly and quickly return to the real value.

The response curves of states p_1, p_2 and P_c are shown in Figures 5-7 when applying the control methods proposed in this paper and the control methods described in reference (21). It can be observed that both control methods have achieved tracking of the setpoints for states p_1, p_2 and P_c. When a LOE fault occurs in the system within 15s, the response curve in reference (21) will exhibit significant jumps. However, due to the strong robustness of adaptive sliding mode control and H_∞ control, coupled with the capability of the proposed method to estimate the fault coefficient, the response curve in this paper is almost unaffected. Furthermore, from the zoomed-in view on the graph, it can be observed that when the system state approaches the setpoint,

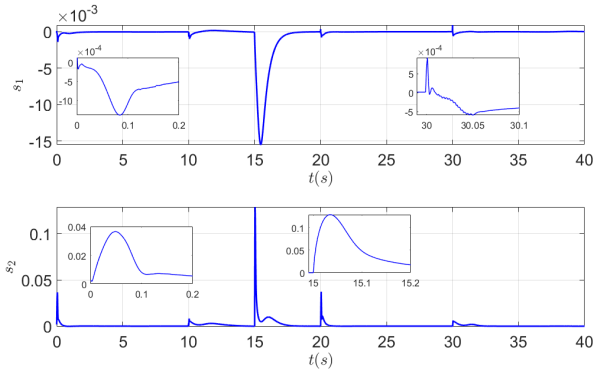

FIGURE 3 Response curve of sliding mode surface

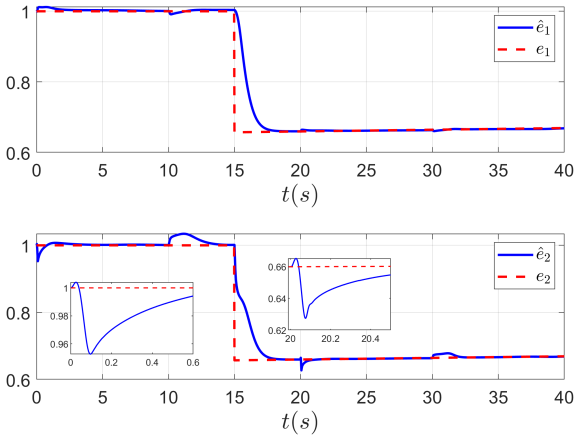

FIGURE 4 Estimation of LOE faults

the response curve of the method proposed in reference (21) exhibits noticeable chattering phenomenons, and there is a small residual error compared to the control setpoint. Additionally, when the system state transitions, the response curve of the method in (21) (especially for state P_c) exhibits significant overshoot.

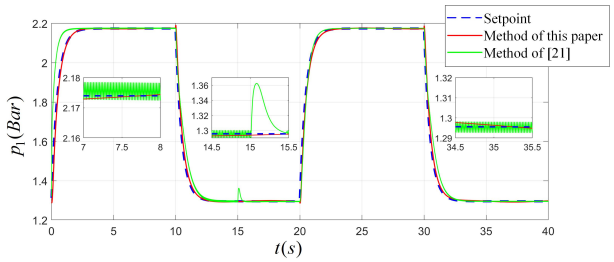

FIGURE 5 Response curve of p_1

Compare to (21), the control algorithm proposed in this paper can accurately control the system states, and at the same time realize the accurate estimation of the LOE fault value. The estimated results can be used as an effective basis for evaluating the health status of actuators. If the LOE value is too small, it means that the actuator has a large hidden danger, and the actuator can be repaired or replaced.

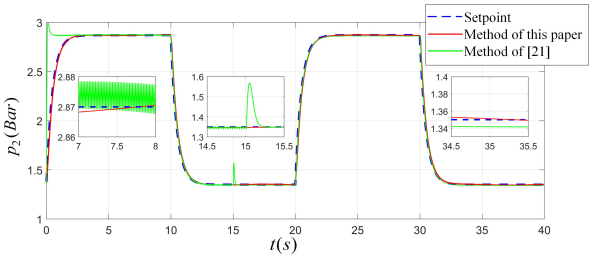

FIGURE 6 Response curve of p_2

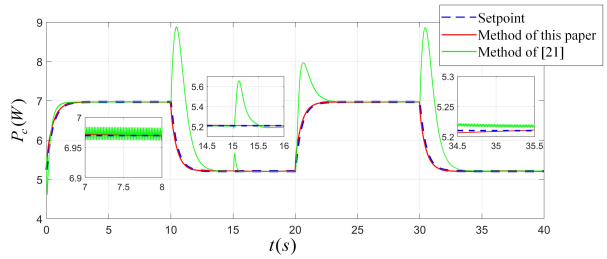

FIGURE 7 Response curve of P_c

TABLE 3 Comparison of different methods in handling bad effects for the DEAP system

Bad Effects	(18)	(17)	(19)	(21)	This Paper
Matched Disturbances	×	×	✓	✓	✓
Mismatched Disturbances	×	×	✓	×	✓
LOE Faults	×	✓	×	✓	✓
Additive Faults	✓	✓	✓	✓	✓

The control input curve is depicted in Figure 8. It is evident that, apart from a minor jump in the input during state switches, the input curve remains consistently smooth throughout other instances.

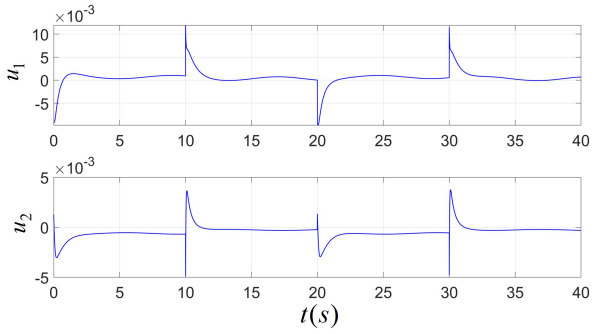

FIGURE 8 Response curve of u

Case 2: Performance of system with actuator faults and mismatched disturbances

To the best of our knowledge, for the DEAP system, the control algorithm proposed in this paper is the first to simultaneously handle additive faults, LOE faults, matched and mismatched disturbances. The advantages of our approach compared to other methods are shown in the Table 3.

In this case, it is assumed that the above bad effects exist simultaneously. First, assume that the sum of external disturbances and additive faults is:

$$D = [0.12\cos(1.2t), 0.1\sin(0.3t), 0.2]^T$$

and the LOE fault is:

$$E(t) = \begin{cases} \mathbf{I}_{2\times 2} & 0 \leq t < 15s \\ 1 - \arctan(5 * (t-15)/70) \times \mathbf{I}_{2\times 2} & 15s \leq t < 25s \\ 1 - \arctan(5 * (25-15)/70) \times \mathbf{I}_{2\times 2} & 25s \leq t \leq 40s \end{cases}$$

As shown, in this case, the system is subjected to mismatched external disturbances and more challenging actuator faults. The response results of system states p_1, p_2 and P_c are depicted in Figure 9-11. The results in this figures demonstrate that, compared to Case 1, the system response is hardly affected even when facing more severe challenges.

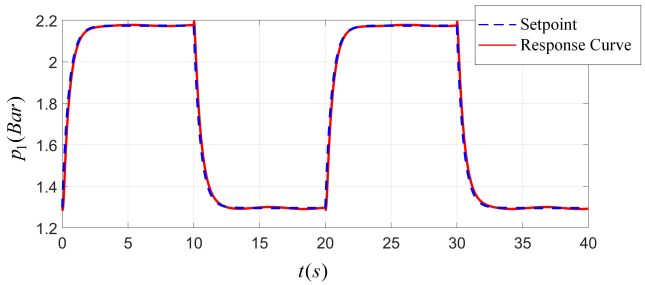

FIGURE 9 Response curve of p_1

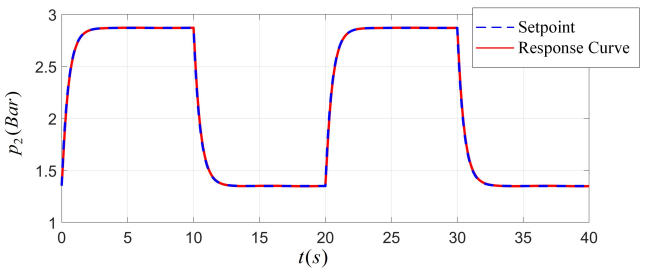

FIGURE 10 Response curve of p_2

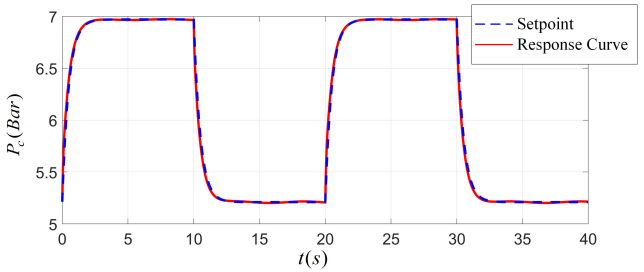

FIGURE 11 Response curve of P_c

The control input curve is depicted in Figure 12. Similar to Case 1, except that the input will jump slightly when the state is switched, the input curve is very smooth at other times.

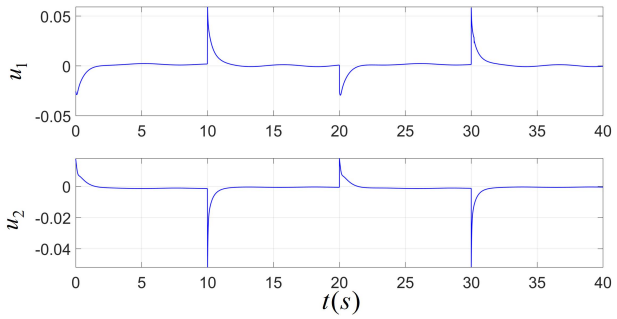

FIGURE 12 Response curve of u

The response of the sliding mode surface is depicted in Figure 13. It can be observed that before the occurrence of the LOE fault, the response curve of the sliding mode surface is nearly identical to that of Case 1, showing no significant chattering. As the LOE coefficient gradually decreases, the sliding mode surface exhibits larger chattering when the system switches state, but it still returns to a stable state within a relatively short time. This indicates that the actuator fault has some impact on the system's response, which is mitigated by the fault-tolerant control algorithm. However, as the fault becomes more severe, measures such as maintenance or replacement of the corresponding actuator are required.

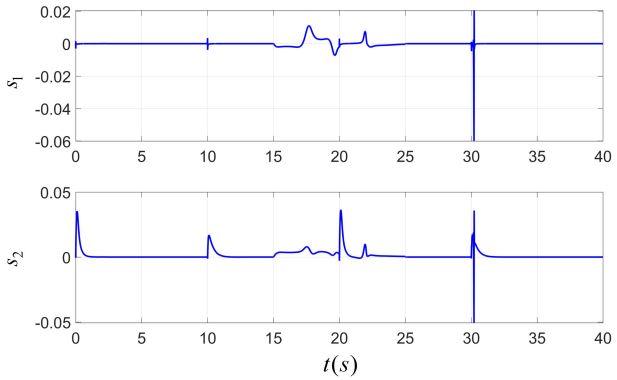

FIGURE 13 Response curve of sliding mode surface

Figure 14 illustrates the real and estimated curves of the LOE coefficients for the actuator. It can be observed that with the adaptive updating algorithm, the current fault coefficients of the actuators can be accurately estimated. Evaluating the fault coefficient of the actuator can serve as a basis for determining whether maintenance of the actuator is required.

The combination D of external disturbance and additive fault can be observed by the disturbance observer, and the response curve of the disturbance observer is shown in the figure 15. It can be seen that the estimated value of the disturbance observer converges to the true value in a short time. When the system state switches, the disturbance observer will jump significantly. According to the analysis of Theorem 1, it can be concluded that the observation error of the disturbance observer has an upper bound and tends to 0, and the simulation results are consistent with the derivation results.

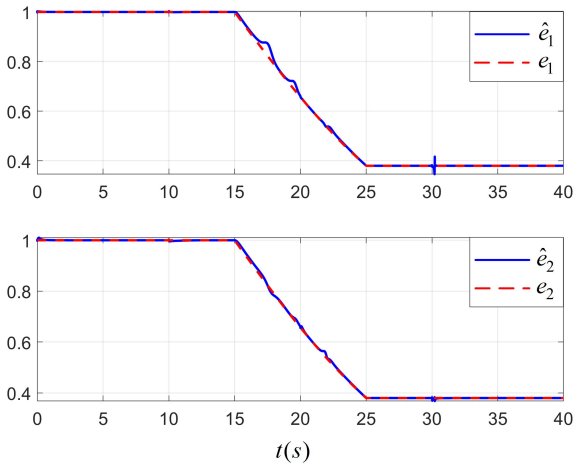

FIGURE 14 Estimation of LOE faults

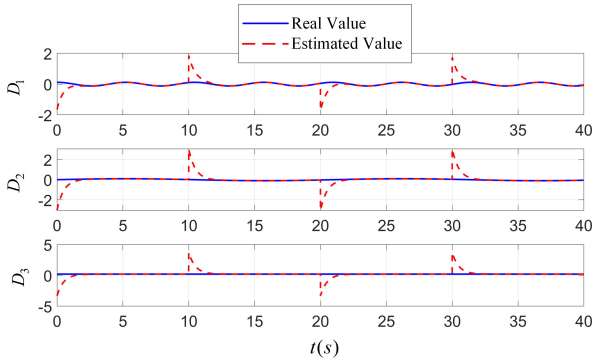

FIGURE 15 Response curve of D

5 | CONCLUSIONS

This paper proposes an adaptive fault-tolerant sliding mode control method for DEAP systems based on the H_∞ theory and disturbance observer. The proposed method can effectively handle both LOE and additive faults occurring in the input variables of the system model caused by faults in the EGR and VGT systems. Additionally, it is capable of addressing matched and mismatched disturbances that the system may encounter. Furthermore, simulation results demonstrate that, compared to other methods, this approach exhibits less sensitivity to faults and external disturbances, resulting in superior response performance when dealing with the same fault-tolerant control problem. Additionally, this method allows for the assessment of the actuator fault coefficient, serving as a basis for deciding whether to perform maintenance on the actuator. Simulation results show that as the actuator fault coefficient decreases, chattering phenomena on the sliding mode surface are still present. Future research will further optimize the design of the controller to address this issue.

DATA AVAILABILITY

The datasets generated during the current study are not publicly available but are available from the corresponding author upon reasonable request.

CONFLICTS OF INTEREST

The authors declare that they have no known competing financial interests or personal relationships that could have appeared to influence the work reported in this paper.

REFERENCES

1. Ni P, Wang X, Li H. A review on regulations, current status, effects and reduction strategies of emissions for marine diesel engines. *Fuel.* 2020;279:118477.
2. Mohamed Shameer P, Ramesh K, Sakthivel R, Purnachandran R. Effects of fuel injection parameters on emission characteristics of diesel engines operating on various biodiesel: A review. *Renewable and Sustainable Energy Reviews.* 2017;67:1267-1281.
3. E J, Pham M, Zhao D, et al. Effect of different technologies on combustion and emissions of the diesel engine fueled with biodiesel: A review. *Renewable and Sustainable Energy Reviews.* 2017;80:620-647.
4. Fayaz H, Mujtaba M, Soudagar MEM, et al. Collective effect of ternary nano fuel blends on the diesel engine performance and emissions characteristics. *Fuel.* 2021;293:120420.
5. Li L, Wang J, Wang Z, Xiao J. Combustion and emission characteristics of diesel engine fueled with diesel/biodiesel/pentanol fuel blends. *Fuel.* 2015;156:211-218.
6. Duan X, Xu Z, Sun X, Deng B, Liu J. Effects of injection timing and EGR on combustion and emissions characteristics of the diesel engine fuelled with acetone–butanol–ethanol/diesel blend fuels. *Energy.* 2021;231:121069.
7. Maiboom A, Tauzia X. NOx and PM emissions reduction on an automotive HSDI Diesel engine with water-in-diesel emulsion and EGR: An experimental study. *Fuel.* 2011;90(11):3179-3192.
8. Rajesh kumar B, Saravanan S. Effect of exhaust gas recirculation (EGR) on performance and emissions of a constant speed DI diesel engine fueled with pentanol/diesel blends. *Fuel.* 2015;160:217-226.
9. Liang J, Zhang Q, Chen Z, Zheng Z, Yang C, Ma Q. The combustion and emission characteristics of diesel-ethanol blends with THF as cosolvents in a diesel engine operating with EGR. *Fuel.* 2021;298:120843.
10. Verschaeren R, Schaepdryver W, Serruys T, Bastiaen M, Vervaeke L, Verhelst S. Experimental study of NOx reduction on a medium speed heavy duty diesel engine by the application of EGR (exhaust gas recirculation) and Miller timing. *Energy.* 2014;76:614-621.
11. Guzzella L, Amstutz A. Control of diesel engines. *IEEE Control Systems Magazine.* 1998;18(5):53-71.
12. Murilo A, Alamir M, Alberer D. A general NMPC framework for a diesel engine air path. *International Journal of Control.* 2014;87(10):2194-2207.
13. Ortner P, Re dL. Predictive Control of a Diesel Engine Air Path. *IEEE Transactions on Control Systems Technology.* 2007;15(3):449-456.
14. Yan F, Wang J. Control of diesel engine dual-loop EGR air-path systems by a singular perturbation method. *Control Engineering Practice.* 2013;21(7):981-988.
15. Mrdjan J, Miroslava J, Kolmanovsky . Constructive Lyapunov control design for turbocharged diesel engines. *IEEE Transactions on Control Systems Technology.* 2000;8(2):288-299.
16. Larguech S, Aloui S, Pagès O, Hajjaji AE, Chaari A. Robust Adaptive Controller for the Diesel Engine Air Path with Input Saturation. *International Journal of Control, Automation and Systems.* 2019;17:2541–2549.
17. Ahmed Ali S, Guermouche M, Langlois N. Fault-tolerant control based Super-Twisting algorithm for the diesel engine air path subject to loss-of-effectiveness and additive actuator faults. *Applied Mathematical Modelling.* 2015;39(15):4309-4329.
18. Hamouda LB, Ayadi M, Langlois N. Fuzzy fault tolerant predictive control for a diesel engine air path. *International Journal of Control Automation and Systems.* 2016;14(2):443-451.
19. Mohamed G, Sofiane AA, Nicolas L. Adaptive super twisting extended state observer based sliding mode control for diesel engine air path subject to matched and unmatched disturbance. *Mathematics and Computers in Simulation.* 2018;151:111-130.
20. Li W, Zhang J, Liu L, Ma X. Finite-Time Fault-Tolerant Control for Diesel Engine Air Path via Extended State Observer. *IEEE Access.* 2019;7:65405-65414.
21. Zhang J, Zhao H, Feng Z, Liu L. Fault-tolerant control for turbocharged diesel engine air path via disturbance observer. *International Journal of Systems Science.* 2021;52(7):1329-1345.
22. Zhang Y, Wang X, Wang S, Miao J. DO-LPV-based robust 3D path following control of underactuated autonomous underwater vehicle with multiple uncertainties. *ISA Transactions.* 2020;101:189-203.

23. Zhang Y, Wang S, Heinrich MK, Wang X, Dorigo M. 3D hybrid formation control of an underwater robot swarm: Switching topologies, unmeasurable velocities, and system constraints. *ISA Transactions.* 2023;136:345-360.
24. Zhang Y, Wang S, Wang X, Tian X. Bearing-based formation control for multiple underactuated autonomous surface vehicles with flexible size scaling. *Ocean Engineering.* 2023;267:113242.
25. Yang X, Wang X, Wang S, Wang K, Sial MB. Finite-time adaptive dynamic surface synchronization control for dual-motor servo systems with backlash and time-varying uncertainties. *ISA Transactions.* 2023;137:248-262.
26. Zhang JH, Liu XW, Xia YQ, Zuo ZQ, Wang YJ. Disturbance Observer-Based Integral Sliding-Mode Control for Systems With Mismatched Disturbances. *IEEE Transactions on Industrial Electronics.* 2016;63(11):7040-7048.
27. Wang Y, Jiang B, Wu ZG, Xie S, Peng Y. Adaptive Sliding Mode Fault-Tolerant Fuzzy Tracking Control With Application to Unmanned Marine Vehicles. *IEEE Transactions on Systems, Man, and Cybernetics: Systems.* 2021;51(11):6691-6700.
28. Li M, Chen X, Liu M, Zhang Y, Zhang H. Asynchronous Adaptive Fault-Tolerant Sliding-Mode Control for T–S Fuzzy Singular Markovian Jump Systems With Uncertain Transition Rates. *IEEE Transactions on Cybernetics.* 2022;52(1):544-555.
29. Liu L, Zhang L, Hou Y, Tang D, Liu H. Implementation of adaptive fault-tolerant tracking control for robot manipulators with integral sliding mode. *International Journal of Robust and Nonlinear Control.* 2023;33(10):5337-5364.
30. Li D, Chen M, Peng K, Wu L. Fixed-time fault-tolerant control of manipulator systems based on sliding mode observer. *International Journal of Robust and Nonlinear Control.* 2023. doi: https://doi.org/10.1002/rnc.6980
31. Wang B, Shen Y, Li N, Zhang Y, Gao Z. An adaptive sliding mode fault-tolerant control of a quadrotor unmanned aerial vehicle with actuator faults and model uncertainties. *International Journal of Robust and Nonlinear Control.* doi: https://doi.org/10.1002/rnc.6631
32. Yao L, Wu Y. Robust fault diagnosis and fault-tolerant control for uncertain multiagent systems. *International Journal of Robust and Nonlinear Control.* 2020;30(18):8192-8205.
33. Larsen M, Jankovic M, Kokotovic P. Indirect passivation design for a diesel engine model. *Proceedings of the 2000 IEEE International Conference on Control Applications.*. 2000:309-314.
34. Zhang J, Wu WJ, Xie WB, Peng C. Dimensional-varying integral sliding mode controller design for uncertain Takagi–Sugeno fuzzy systems. *Information Sciences.* 2021;565:77-90.
35. Li S, Yang J, Chen WH, Chen X. Generalized Extended State Observer Based Control for Systems With Mismatched Uncertainties. *IEEE Transactions on Industrial Electronics.* 2012;59(12):4792-4802.
36. Sai H, Xu Z, Xia C, Sun X. Approximate continuous fixed-time terminal sliding mode control with prescribed performance for uncertain robotic manipulators. *Nonlinear Dynamic.* 2022;110:431-448.